

# AIRLOAD PREDICTIONS FOR DELTA WINGS AT HIGH INCIDENCE

X. Z. Huang, H.Y. Lou and E.S. Hanff

Institute for Aerospace Research, National Research Council of Canada

**Keywords:** *vortex breakdown, aerodynamic load, high incidence*

## Abstract

*An approach based on the application of the Non-Linear Indicical Response method to internal flow state variables, such as vortex breakdown location over a delta wing, is developed to predict the non-linear and time dependent loads acting on the wing undergoing high angular rates at high incidence. By combining experimental, analytical and simple computational approaches this method can be used to predict airloads at the conceptual design stage with a minimum of testing requirements and simple computational work. Additional work is required to further refine the method, which can, in principle, be extended to other situations.*

## 1 Introduction

The tactical advantage enjoyed by more maneuverable and agile fighter aircraft has been an incentive to continually expand their flight envelope. Under advanced maneuvering conditions, however, the flow around the aircraft is very complex leading to highly non-linear and time dependent airloads. Adequate aerodynamic models are essential for flight mechanics predictions in that regime, where conventional locally linear modeling has been shown to be incapable of reflecting the actual airloads. On the other hand, the Non-linear Indicical Response (NIR) method developed by Tobak et al.<sup>1,2</sup> provides a theoretical mathematical framework for the required modeling. The method is based on the application of the generalized superposition integral to the Frechet derivative of the airload functional, thus allowing the prediction of the load for arbitrary motion histories. The integral must be split at critical states where Frechet

differentiability is lost. The existence of multiple critical states renders the application of the method to predict loads directly from the motion variables very difficult.

However, physical considerations permit identifying the critical states with the most impact, for example, in the case of vortex dominated flows over sharp leading-edge delta wings, there are four different flow states depending on attitude: fully intact leading-edge vortex, vortex breakdown, spiral flow (breakdown at apex) and large-scale turbulence flow at very high incidence. Vortex breakdown is known to be the main cause of airloads non-linearities and time dependence. As a consequence, prediction of breakdown location over the wing is a logical first step in predicting airloads. The NIR method can be used rather readily to do so in terms of the motion variables, as no critical states are encountered in this state-space, provided breakdown is on the wing. Once the breakdown location is known, it is possible to calculate airloads by a simple computational vortex method described below.

The above methodology is not constrained to the examples discussed here, but can be applied to other cases where dominant effect represented by a characteristic parameter, can be defined, such as flow separation or transition location on airfoil lift, vortex asymmetry on slender bodies loads, etc.

## 2 Dominant effect of vortex breakdown on airloads

The effect of breakdown on aerodynamic loads under both static and dynamic conditions is well recognized. Illustration of this effect on the rolling moment coefficient of a 65° delta wing (Fig. 1) at a body axis inclination  $\sigma=30^\circ$  under

static and dynamic conditions are shown in Fig. 2 and Fig. 3 respectively<sup>3,4</sup>. The experimentally observed rolling moment is compared with a hypothetical one that assumes an intact vortex on the leeward wing half and breakdown at the apex on the windward wing half. Solid symbols indicate that this condition is satisfied, whereas clear ones indicate that breakdown is present over at least one wing half.

Important discrepancies between the curves exist in the presence of breakdown over the wing. Fig. 3 shows the corresponding curves for roll oscillation cases with the same amplitude and varying frequency. The very slow breakdown propagation speed (an order of magnitude slower than convection speed) causes increasing phase shifts at the higher frequencies.

Similar phenomena are observed in the pitching case<sup>5</sup>. Fig. 4a and Fig 4c show the normal force acting on the same model during transient pitch-up and pitch-down motions between 0 and 60° respectively (Fig. 4b and Fig. 4d). The corresponding static normal force is superimposed for comparison. The vortex breakdown locations for these motions are depicted in Fig. 5 where point A to point B is breakdown region (from a kink point to large-scale turbulence). The static locations are also included. By connecting with Fig. 5, it can be observed in Fig. 4 that when breakdown crosses the trailing edge onto the wing there is only a small reduction in the slope of the experimental. This is in agreement with the above rolling observations and with Kegelman and Roos' experiments<sup>6</sup> to investigate the effect of breakdown location on airloads where they found that "the effect of shifting the burst point by as much as 40% chord from trailing edge is indeed small ( $\Delta C_L/C_L \approx 0.05$ )". However, when breakdown reaches the apex at  $\alpha \approx 46^\circ$ , the flow changes from spiral to large-scale turbulent resulting in a dramatic and almost discontinuous drop in normal force. The difference between the static and dynamic curves is clearly the result of the significant delays in breakdown location depicted in Fig. 5.

The above observations cover four flow states: vortical flow, vortex breakdown flow, spiral flow and large-scale turbulent flow

depending on the motion variables and their history. Important critical states are associated with changes between these flow states, namely when breakdown reaches the apex and crosses the trailing edge. Given the importance of breakdown on the loads it is necessary to determine its location as a first step in predicting airloads.

### 3 Circulation criterion for the prediction of leading-edge vortex breakdown

Leading-edge vortex breakdown is determined by the balance between the vorticity feeding rate at the leading-edge boundary-layer separation and the vorticity convection rate downstream due to the pressure gradient. If the former is larger than the latter, there is an increase in negative azimuthal vorticity associated with a tilting of the vortex core that causes a reduction of the axial velocity which further increases the tilt and so on<sup>7,8</sup>. This feedback process continues until the axial velocity approaches zero, corresponding to the breakdown of the vortex. As a general rule, the relative importance of the two effects can be represented by the swirl parameter  $S$ , or Rossby number  $R$ , where  $S$  and  $R$  are defined as:

$$S = \frac{\Gamma}{D_c U_{x(\text{axis})}} = \frac{l}{2R} \quad (1)$$

Theoretical and numerical values of the critical swirl parameter  $S^*$  at which breakdown occurs are given in the following table which is taken from Ref. 9 but with  $D_c$  as a reference length. It shows that the various approaches lead to similar results. The differences can be partly due to different assumptions regarding the adverse pressure gradients<sup>9</sup>.

Sources	$S^*$
Quasi Cylin. approx.	0.705
Axisym. N.-S.	0.675
Bossel	0.56
Squire	0.7
Benjamin	0.7
Num.simul.	0.64
Spall	0.68

In the case of an intact vortex over a delta wing, Eqn. (1) becomes:

$$S = \frac{\Gamma(\alpha, \Lambda)}{c \cdot U_{x(\text{axis})}(\alpha, \Lambda)} \leq S^* \quad (2)$$

where  $\Lambda$  is half apex angle and  $c$  is center chord. By substituting  $U_\infty$  for  $U_{x(\text{axis})}$  Eqn.(2) could be rewritten as:

$$\bar{\Gamma}(\alpha, \Lambda, x) = \frac{\Gamma(\alpha, \Lambda, x)}{cU_\infty} \leq \Gamma^*(\alpha, \Lambda) \quad (3)$$

where

$$\Gamma^*(\alpha, \Lambda) = S^* \left( \frac{U_x}{U_\infty} \right) \quad (4)$$

Eqn.(3) shows that when the local non-dimensional circulation parameter reaches a certain critical value, the vortex breaks down.

Based on Hemsch and Luckring's finding<sup>10</sup> that the circulation in the wake of a delta wing is a function of angle-of-attack and sweep only, the following simple relationship was developed that provides results in good agreement with theirs:

$$\bar{\Gamma}_{x \geq l} = 5.11 \cdot (\Lambda + \Delta\Lambda) \cdot (\alpha - \Delta\alpha) \quad (5)$$

The chordwise distribution of circulation still needs to be established. A conical model adopted by researchers in the past<sup>11,12</sup> requires a conical flow with a constant axial pressure gradient that does not exist on a delta wing due to the effect of the trailing edge which causes a variable adverse pressure gradient over the length. It is therefore necessary to develop a model for the circulation that accounts for this effect. Experimental results<sup>13</sup> and CFD calculations for NS equations<sup>14</sup> show that the circulation along the chordwise direction of delta wings exhibits non-linear characteristics (Fig. 6). Based on these observations the circulation distribution is assumed to have a parabolic form:

$$\bar{\Gamma}(\alpha, \Lambda, x) = C_0 + Bx - Ax^2 \quad (6)$$

where  $A$  and  $B$  are given by:

$$A = 1.1 \cdot \sin \alpha \cdot \sin \Lambda$$

$$B = 4A$$

and  $C_0$  is the circulation at the apex. The requirement for a finite  $C_0$ , frequently assumed to be zero, arises from the fact that in the latter case breakdown would never reach the apex,

which is demonstrably not the case. A possible explanation for the existence of  $C_0$  at the apex is the fact that the attachment node is located somewhat aft of the apex proper on the windward side and some vorticity is generated due to boundary layer separation in that region.  $C_0$  is given by:

$$C_0 = \bar{\Gamma}_{x=l}(\alpha, \Lambda) - B + A$$

and the breakdown location can be obtained by:

$$C_0 + Bx_{VB} - Ax_{VB}^2 = \Gamma^*(\alpha, \Lambda) \quad (7)$$

$\Gamma^*(\alpha, \Lambda)$  is based on the critical value of the Rossby number  $S^*$  modified to account for the velocity component along the vortex axis and the interaction between the vortices on both wing halves, leading to:

$$\Gamma^*(\alpha, \Lambda) = 0.78 \cdot \cos(4(\Lambda - \Lambda_0))$$

where  $\Lambda_0$  is the optimum half apex angle ( $\Lambda_0 \approx 19.5^\circ$ ). The calculated chordwise distribution of the non-dimensional circulation for delta wings with different sweep angles at  $\alpha = 26^\circ$  and a  $65^\circ$  delta wing at various angles of attack are shown in Fig. 7a and Fig. 7b respectively. While Fig. 7c is predicted vortex breakdown locations for sharp-edged delta wings with sweep angles ranging from  $60^\circ$  to  $80^\circ$  in the pitch case.

The comparisons between predicted and experimental results are shown in Fig. 8. The experimental values were obtained by various researchers under different test conditions, explaining some of the scatter. For example Wentz's data for sweepback angle  $\Psi \geq 70^\circ$  are affected by aeroelastic deformations of the thin model used, whereas Lambourne's data were obtained under rather high blockage conditions. Given the complexity of the vortex breakdown process and its sensitivity to test conditions, the comparisons are reasonable.

#### 4 Roll rate induced camber and motion history effects

When the wing is rolling about its body axis, the roll rate induced "section angle" increment,  $\Delta\alpha_s$ , along the leading-edge and chordwise angle of attack increment,  $\Delta\alpha_c$  are<sup>15</sup>

$$\Delta\alpha_s = \cos^{-1}\left(\frac{\dot{\phi} \cdot y}{U_s}\right)$$

$$\Delta\alpha_c = \cos^{-1}\left(\frac{\dot{\phi} \cdot y}{U_c}\right)$$

where  $U_C$  and  $U_S$  are the freestream velocity components in the chordwise direction and normal to the leading edge respectively. In general, these changes in angles are denoted roll-rate induced camber effects. Since the instantaneous camber changes the condition of boundary layer separation, it induces incremental vorticity feeding and convection rates, either positive or negative depending on the motion. If there is no time lag, these quantities are added to the previous static solution as a quasi-steady effect. The long response time of the breakdown location to perturbations must be included as a motion history effect. In the absence of critical states, the NIR method can be readily applied to define the instantaneous location of breakdown:

$$\bar{x}_{vB} = X_1(\phi(t)) + X_2(\dot{\Phi}(t)) \cdot X_1(\phi(t)) + \int_0^T X_3(t-\tau)\Phi(\tau)d\tau \quad (8)$$

The first term on the RHS of Eqn (8) represents the static location, the second one the quasi-steady (camber) effect and the third one the unsteady (motion history) effect in the form of a convolution integral and

$$X_2(\dot{\Phi}(t)) = \frac{0.9I}{\tan\alpha(t)}\dot{\Phi}(t)$$

$$X_3(t) = k \sin\frac{\pi}{T^*} \quad \text{for } 0 < t < T^*$$

$\dot{\Phi}$  is the reduced angular rate,  $T^*$  is the time lag of vortex breakdown and  $k$  is a constant<sup>16</sup>.

Comparisons between predicted and observed breakdown locations as a function of roll angle under static and harmonic motion conditions for various reduced frequencies are shown in Fig. 9 where the effective angle of attack, caused by leading-edge bevel, was taken into account. Again, the predictions are reasonable good.

## 5 Aerodynamic loads and surface pressure predictions

Given that the vortex breakdown location has a dominant effect on the airloads, the predicted instantaneous vortex breakdown locations are used to estimate the airloads acting on the wing. Two approaches have been developed depending on the requirements. If only the normal force is needed, a generalized leading-edge suction analogy is used, whereas if surface pressures and other aerodynamic loads are required, a simplified computational vortex method is employed.

In the first method, the airloads are assumed to be made up of a potential and a vortical component as suggested in Polhamus' leading-edge suction analogy<sup>17</sup>

$$C_L = C_{LP} + C_{LV} = K_p \cdot \sin\alpha \cdot \cos^2\alpha + K_v \cdot \cos\alpha \cdot \sin^2\alpha \quad (9)$$

where  $K_p$  and  $K_v$  are defined as:

$$K_p = \frac{2\pi}{1 + \cot\Lambda} \quad \text{and} \quad K_v = \pi \cdot \cos\Lambda$$

The latter is applicable for  $\Lambda \leq 45^\circ$  given that the critical swirl parameter  $S^* \approx \cos 45^\circ$ . Physical explanations of the slight changes in  $K_p$  and  $K_v$  from Polhamus' expressions are given elsewhere<sup>18</sup>. In the presence of breakdown this approach is used in the area upstream of breakdown, whereas downstream of breakdown the vortical term does not disappear immediately but decays exponentially<sup>4</sup>. Under dynamic conditions the airloads are computed on the basis of the instantaneous predicted breakdown locations. By incorporating the instantaneous position of breakdown, airloads nonlinearities and time dependence are automatically accounted for.

Normal force coefficients have been calculated for a large number of static and roll-oscillation conditions. Fig. 10 shows the measured and calculated lift coefficient for delta wings with sweep angle ranging from  $55^\circ$  to  $80^\circ$  at angles of attack up to  $80^\circ$  as well as Polhamus' predictions. As can be observed, the

present method is capable of predicting the normal force even in the presence of breakdown. Furthermore, it has been applied to estimate the normal force in the presence of sideslip and under rolling oscillatory conditions as shown in Fig. 11.

The second and more general method is used for predicting the surface pressure and aerodynamic loads. The effects of secondary and tertiary vortices have been neglected in the present investigation. However the formulation incorporates the primary vortex breakdown over the wing and permits various model motions. Since the circulation distribution is obtained as mentioned above and the vortex core location is obtained empirically or analytically<sup>19,20</sup>, the vortex induced velocity components can be approximately estimated by integrating the contribution from each segment of the vortex filament on the surface with the appropriate boundary conditions. Using vector notation the local velocity due to one vortex is given by

$$\vec{U} = \begin{pmatrix} u \\ v \\ w \end{pmatrix} = \frac{\bar{\Gamma}}{4\pi} \frac{\vec{r}_1 \times \vec{r}_2}{|\vec{r}_1 \times \vec{r}_2|^2} \vec{r}_0 \cdot \left( \frac{\vec{r}_1}{r_1} - \frac{\vec{r}_2}{r_2} \right) \quad (10)$$

where  $\bar{\Gamma}$  is the average strength of the intact vortex between two ends of  $\vec{r}_1$  and  $\vec{r}_2$ .

Therefore the total induced velocity due to the left and right intact vortices at point (P) on the wing surface becomes:

$$\vec{U}_{total} = \begin{pmatrix} u \\ v \\ w \end{pmatrix}_{total}^{(p)} = \sum_{i=1}^n \vec{U}_i^{(p)} + \sum_{j=1}^m \vec{U}_j^{(p)}$$

where  $n$  is the number of vortex segments on the left side and  $m$  on the right one.

Once the velocities over the surface are known, the surface pressure coefficient  $C_p$  can be estimated approximately by:

$$C_{p,Z=0} = -2 \frac{u}{U_\infty} - \frac{v^2}{U_\infty^2} + C_{pp}$$

where  $C_{pp}$  is the potential component.

As examples of the application of the method, the predicted surface pressures at  $x=0.75$  of the  $65^\circ$  delta wing at  $\sigma=30^\circ$  and  $\phi=0^\circ$ ,  $-5^\circ$ , and  $-7^\circ$  are shown in Fig. 12 together with experimental measurements and the time

average of N-S time-dependent solutions<sup>14</sup>. It should be noted that although the latter are too low, the experimental points are well within the range of the unsteady solutions. Details of surface pressures (top and 3D views) over the complete  $65^\circ$  delta wing at various roll angles are shown in Fig. 13. In general the predicted pressure distributions in Fig. 12 are close to the measurements, especially on the leeward wing half. On the windward wing half, however, the measured pressure exhibits a flatter peak than the calculated one. This is due to the fact that although the vortex strength is suitably reflected in the vortex filament model, the increase in the diameter of the spiral flow aft of breakdown and the effect of secondary vortex are not taken into account in the predictions. Additional work is under way to refine the model.

## 6 Conclusions

- The NIR method has been successfully used in conjunction with experimental results, to predict the breakdown location of leading-edge vortices on a delta wing under static and dynamic conditions.
- The predicted breakdown locations can be used as inputs for determining airloads. In the case of normal force, a model based on an extension of the "leading-edge suction analogy" can be used, whereas a simple vortex filament computational model is used for the determination of surface pressures and loads.
- Advantage was taken of the extensive experimental data base available, to develop simple models to handle complex aerodynamics under a variety of situations.
- Additional work is required to refine the proposed methods.

## 7 References

- [1] Tobak, M., Chapman, G.T., and Schiff, L.B. Mathematical Modeling of the Aerodynamic Characteristics in Flight Dynamics, NASA TM 85880, 1984.
- [2] Tobak, M. and Chapman, G.T., Nonlinear Problems in Flight Dynamics Involving Aerodynamic Bifurcations NASA TM 86706, 1985.

[3] Hanff, E.S. and Jenkins, S., Large-Amplitude High-Rate Rolling Experiments on a Delta and Double Delta Wing AIAA Paper 90-0224, 1990.

[4] Huang, X.Z. and Hanff, E.S., Prediction of Normal Force on a Delta Wing Rolling at High Incidence AIAA Paper 93-3686, 1993.

[5] Hanff, E.S. and Huang, X.Z., Rolling and Pitching Experiments on Configurations with a 65° Delta Wing at High Incidence NRC/IAR LTR-A-013.

[6] Kegelman, J., and Roos, F., Effects of Leading-Edge Shape and Vortex Burst on the Flowfield of a 70 Degree Sweep Delta-Wing AIAA Paper 89-0086, 1989

[7] Lopez, J. M., Axisymmetric Vortex Breakdown part 1. Confined Swirling Flow Journal of Fluid Mechanics, 221:533-552, 1990.

[8] Brown, G. L. and Lopez, J. M. Axisymmetric Vortex Breakdown part 2. Physical Mechanisms Journal of Fluid Mechanics, 221:553-576, 1990.

[9] Delery, J.M., Aspects of Vortex Breakdown Prog. Aerospace Sci. Vol. 30, pp. 1-59, 1994.

[10] Hemsch, M., and Luckring, J., Connection Between Leading-Edge Sweep, Vortex Lift, and Vortex Strength for Delta Wings J. Aircraft, Vol. 27, No. 5 May 1990.

[11] Ravindra, K., A Simple Criterion for Vortex Breakdown AIAA Paper 95-2311, 1995.

[12] Jumper, E.J., Nelson, R.C. and Cheung, K., A Simple Criterion for Vortex Breakdown AIAA Paper 93-0866, 1993.

[13] Nelson, R.C., and Visser, K.D., Breaking Down the Delta Wing Vortex AGARD Symposium on Vortex Flow Aerodynamics, Oct. 1990.

[14] Chaderjian, N. and Schiff, L., Navier-Stokes Analysis of a Delta Wing in Static and Dynamic Roll AIAA Paper 95-1868, 1995.

[15] Huang, X.Z. and Hanff, E.S., Roll Rate Induced Camber Effect on Delta Wing Leading-Edge Vortex Breakdown AIAA Paper 95-1793, 1995.

[16] Huang, X.Z. and Hanff, E.S., Prediction of Normal Force on a Delta Wing Rolling at High Incidence AIAA Paper 93-3686, 1993.

[17] Polhamus, E.C., A Concept of the Vortex Lift of Sharp-Edge Delta Wings Based on A Leading-Edge-Suction Analogy NASA TN D-3767, 1966.

[18] Lou, H.Y. Huang, X.Z. and Hanff, E.S., Modified Leading-Edge Suction Analogy To be published

[19] Brown, C.E. and Michael, W.H. Jr., On Slender Delta Wings with Leading-Edge Separation NACA TN 3430, 1955.

[20] Smith, J.H.B., Improved Calculations of Leading-Edge Separation from Slender, Thin, Delta Wings Proc. Roy. Soc. A Vol. 306, 1968.

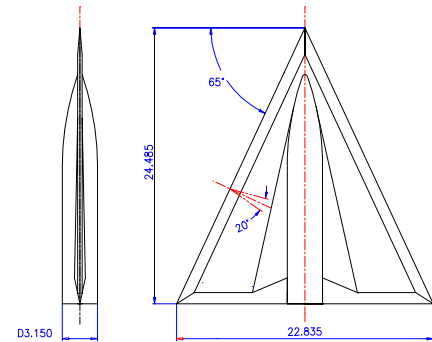


Fig. 1 65° delta wing model

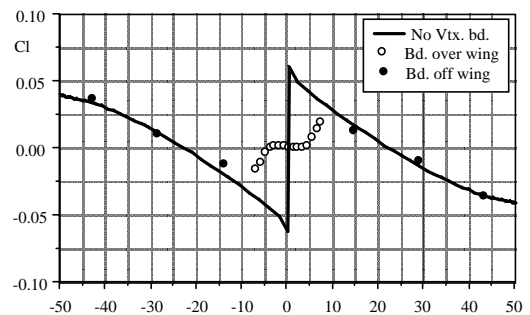


Fig. 2 Effect of vortex breakdown on rolling moment in dynamic case ( $\sigma=30^\circ$ ,  $\Lambda= 65^\circ$ )

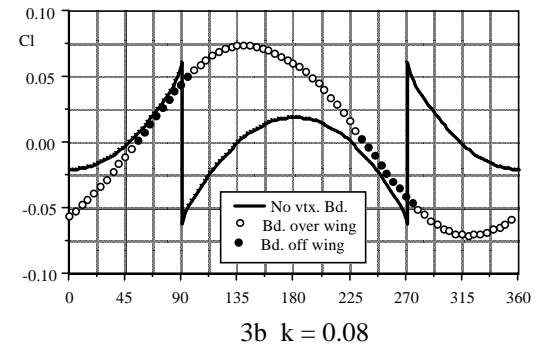
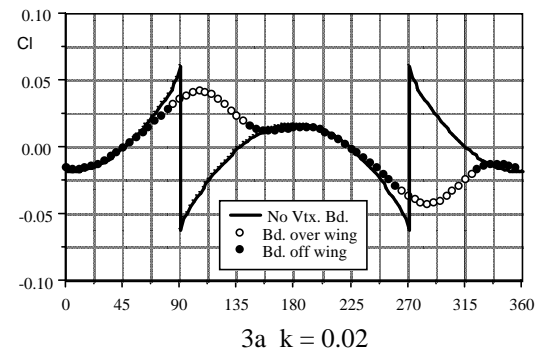


Fig. 3 Effect of vortex breakdown on rolling moment in dynamic case ( $\sigma=30^\circ$ ,  $\Lambda= 65^\circ$ )

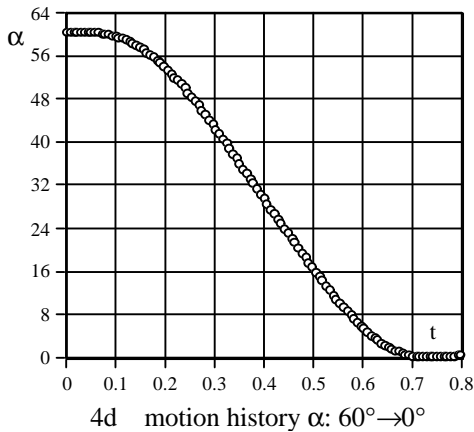
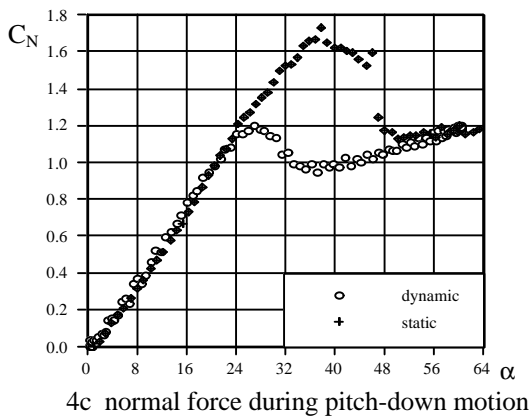
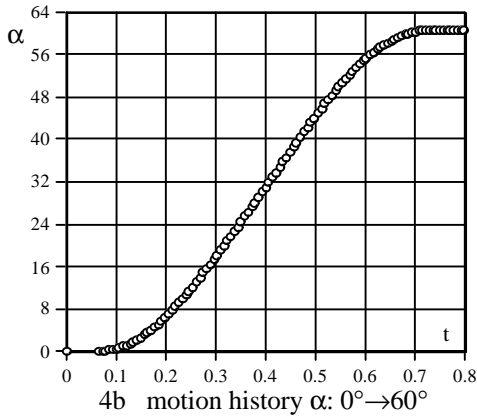
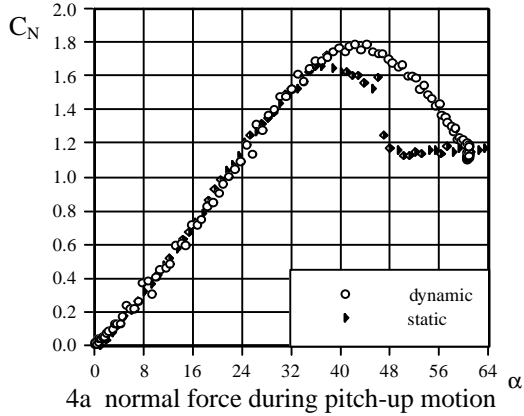


Fig. 4 Normal force during pitch-up and pitch-down motions

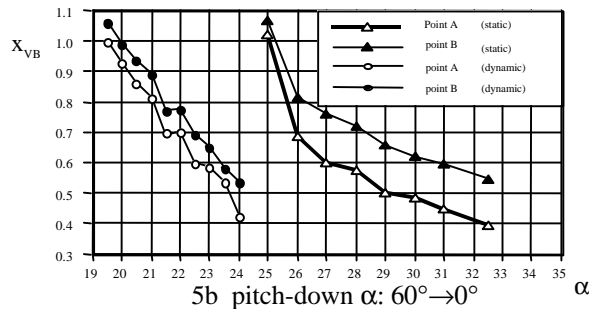
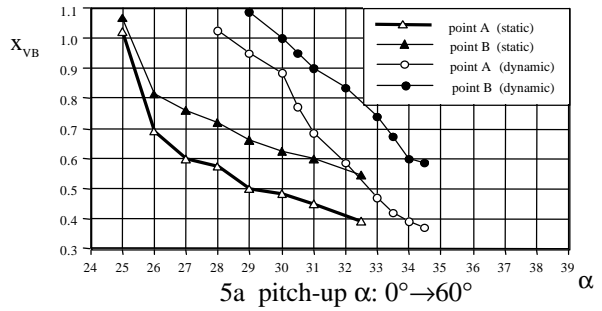


Fig. 5 vortex breakdown locations

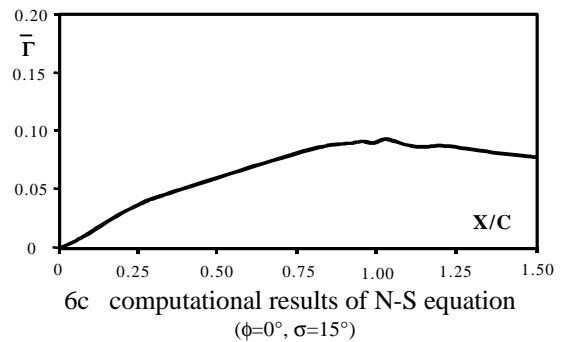
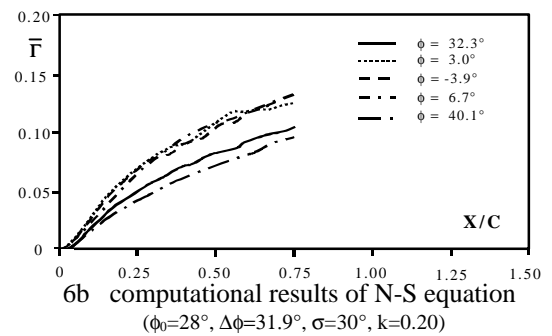
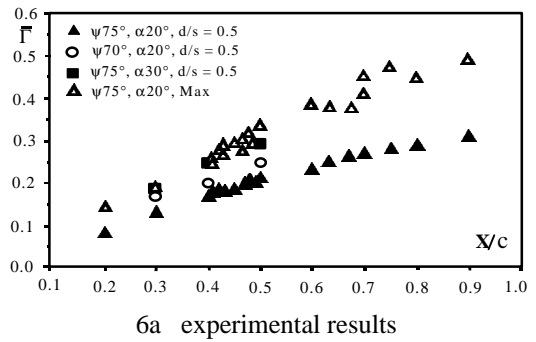


Fig. 6 Chordwise circulation distribution

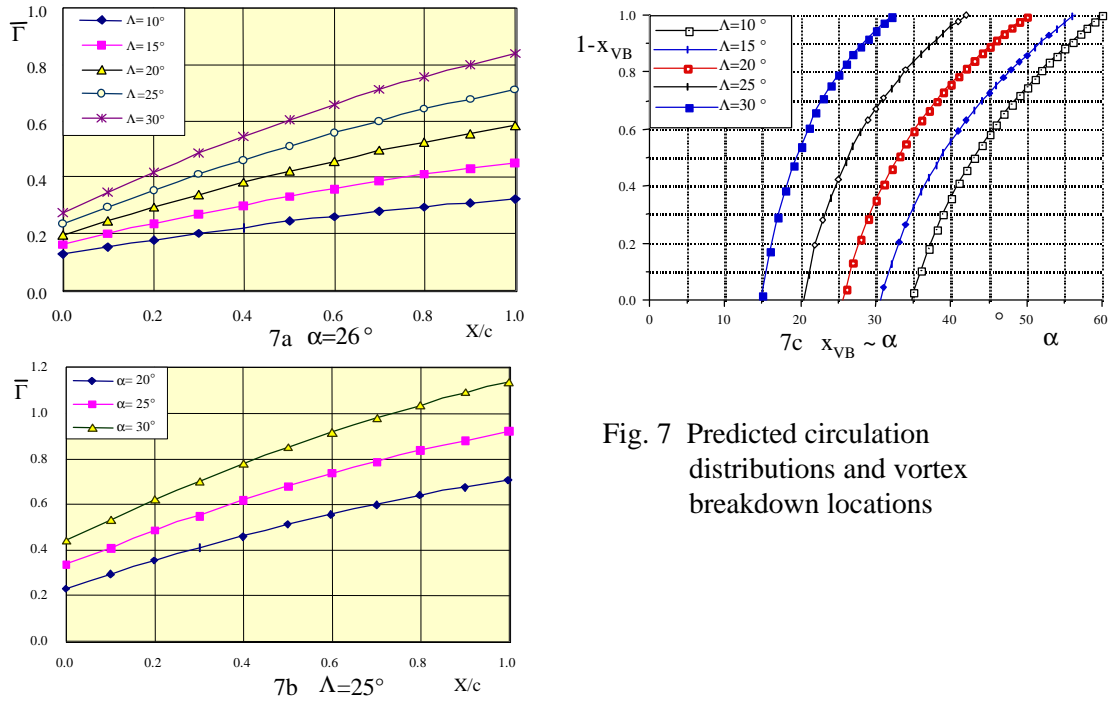


Fig. 7 Predicted circulation distributions and vortex breakdown locations

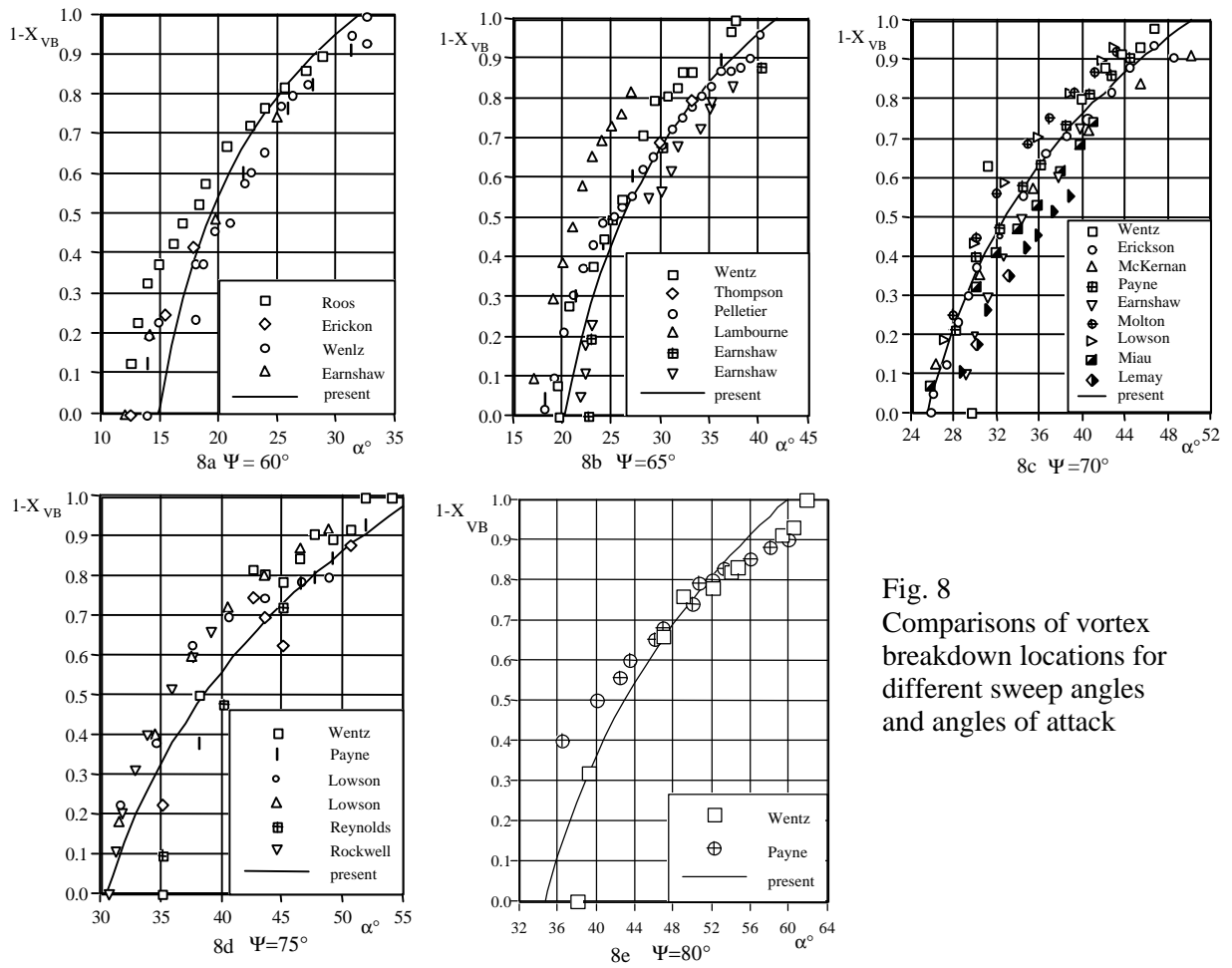


Fig. 8 Comparisons of vortex breakdown locations for different sweep angles and angles of attack

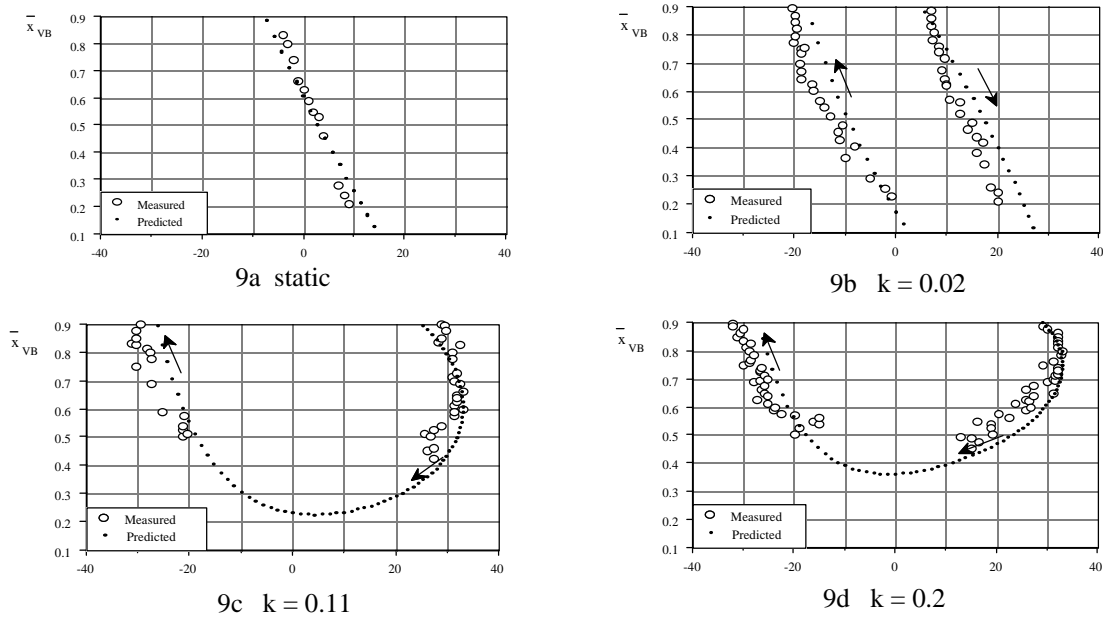


Fig. 9 Predicted and measured breakdown locations for rolled  $65^\circ$  delta wing ( $\sigma=30^\circ$ )

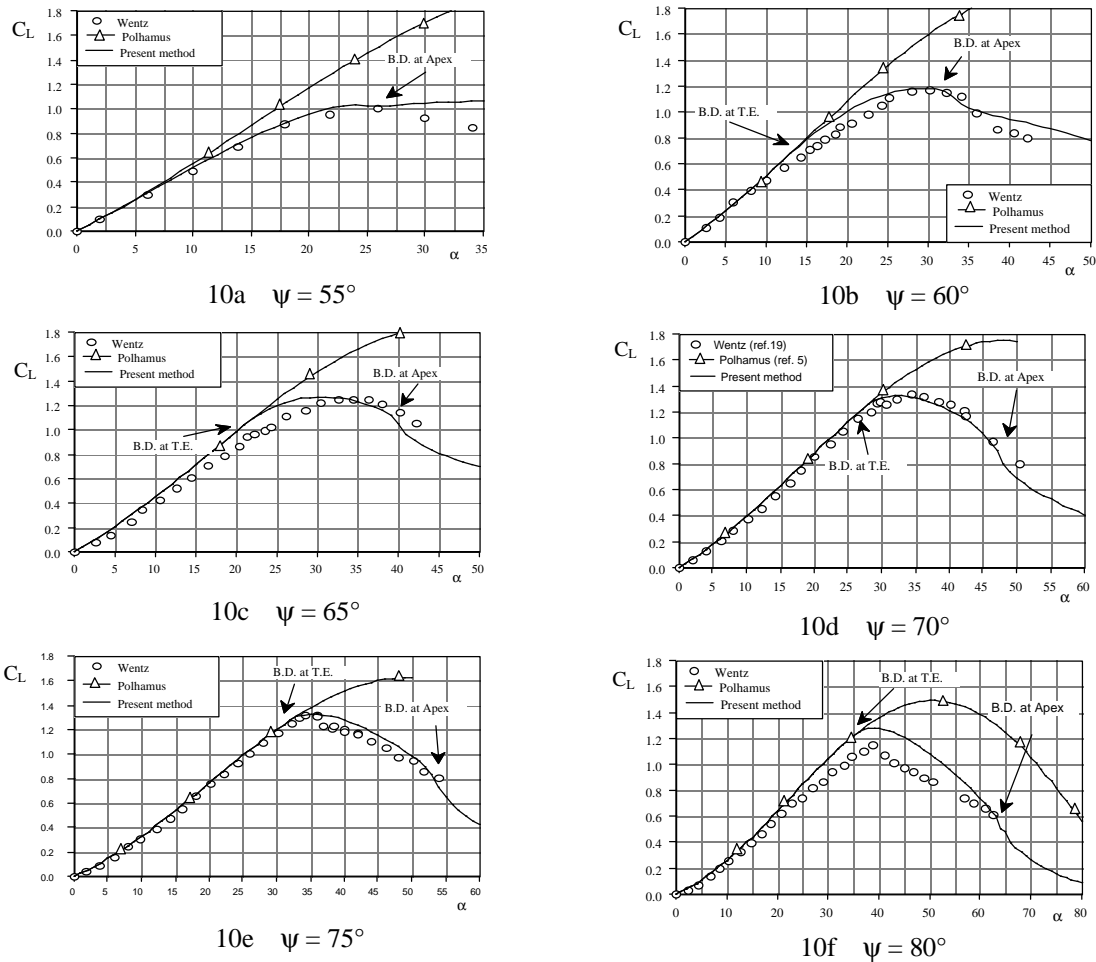


Fig. 10 Static lift coefficient for delta wings with different sweep angles

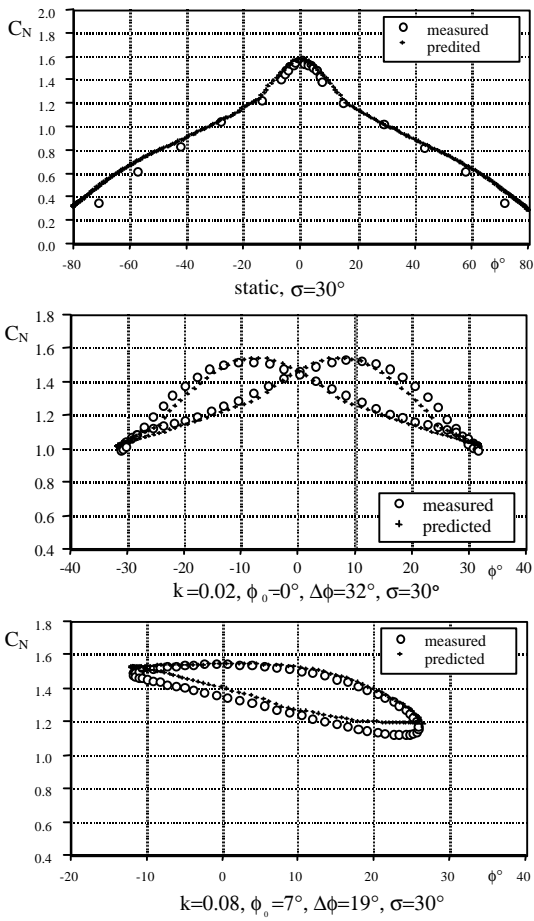


Fig. 11 Comparisons of normal force at static and rolling oscillation condition

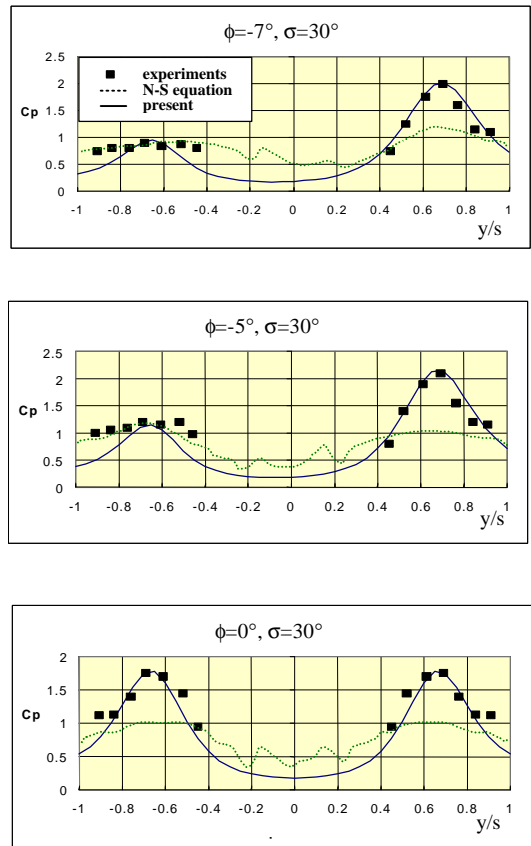


Fig. 12 Comparisons of pressure coefficient for different static conditions ( $\sigma=30^\circ, x/c=0.75$ )

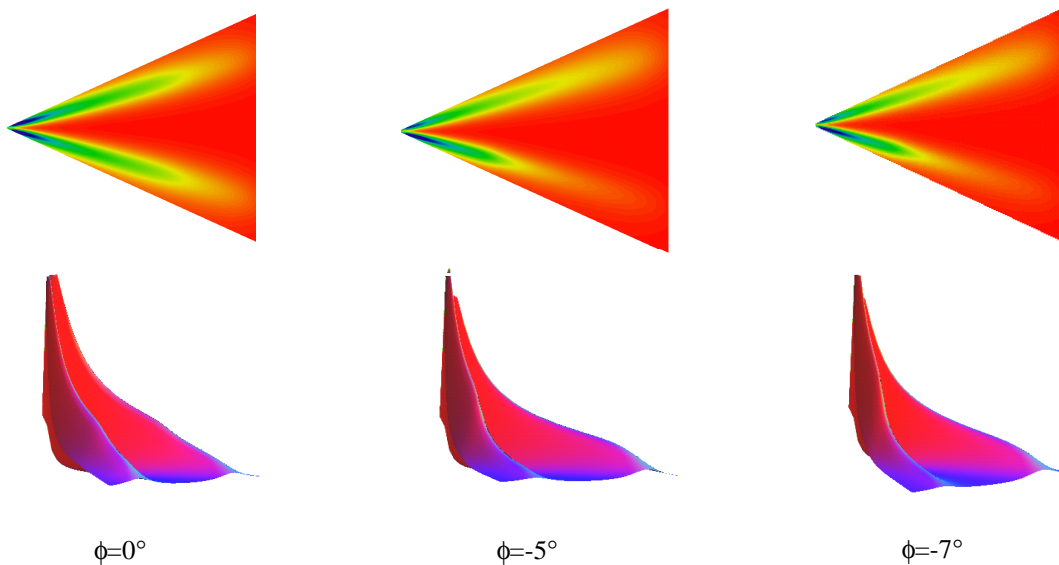


Fig. 13 Top views and 3-D views of predicted surface pressure at different roll angles ( $\sigma=30^\circ$ )